What can we learn from observed temperature and salinity isopycnal anomalies at eddy generation sites? Application in the Tropical Atlantic Ocean

Aguedjou H. M. A.[1,2,*], A. Chaigneau[1,3,2], I. Dadou[1], Y. Morel[1], C. Pegliasco[4], C. Y. Da-Allada[3,5], E. Baloïtcha[2]

[1] LEGOS, University of Toulouse, CNRS, IRD, CNES, UT3, Toulouse, France

[2] CIPMA/UAC, Cotonou, Benin

[3] IRHOB, Cotonou, Benin

[4] CLS, Ramonville Saint-Agne

[5] UNSTB, Abomey, Benin

[*] micael.aguedjou@legos.obs-mip.fr, aguhabib2000@gmail.com

Key points:

- At their generation site, ~50% of observed eddies have non-significant isopycnal temperature/salinity anomalies in the TAO.
- Anticyclonic and cyclonic eddies having significant isopycnal temperature/salinity anomalies can exhibit both positive and negative anomalies.
- Frictional effects play a major role for eddy potential vorticity anomaly generation in the TAO, followed by isopycnal advection and diapycnal mixing.

Abstract:

Potential vorticity (PV) is a key parameter to analyze the generation and dynamics of oceanic mesoscale eddies. Adiabatic and diabatic processes can be involved in the generation of localized PV anomalies and vortices. However, PV is difficult to evaluate at mesoscale. In this study we argue that eddies created by diapycnal mixing or isopycnal advection of water-masses are associated with PV anomalies and significant isopycnal temperature/salinity anomalies (Θ'/S'). In contrast, eddies created by friction are associated with PV anomalies but with non-significant isopycnal Θ'/S'. Based on 18 years of satellite altimetry data and vertical Θ/S profiles from Argo floats, we analyze the isopycnal Θ'/S' within new-born eddies in the tropical Atlantic Ocean (TAO) and discuss the possible mechanisms involved in their generation. Our results show that on density-coordinates system, both anticyclonic (AEs) and cyclonic (CEs) eddies can exhibit positive, negative or non-significant isopycnal Θ'/S'. Almost half of the sampled eddies do not have significant Θ'/S' at their generation site, suggesting that frictional effects play a significant role in the generation of their PV anomalies. The other half of eddies, likely generated by diapycnal mixing or isopycnal advection, exhibits significant positive or negative anomalies with typical Θ' of ±0.5°C. More than 70% of these significant eddies are subsurface-intensified, having their cores below the seasonal pycnocline. Refined analyses of the vertical structure of new-born eddies in three selected subregions of the TAO, show the dominance of cold (warm) subsurface AEs (CEs) likely due to isopycnal advection of large scale PV and temperature.

Keywords: mesoscale eddies; isopycnal temperature/salinity anomalies; eddy generation mechanisms; potential vorticity; tropical Atlantic Ocean.

Plain Language Summary

Mesoscale eddies are common features in the global ocean, having typical length scales of 10 to 100 km and lifespans from days to several weeks. These quasi-circular rotating structures can be formed by several physical processes, such as surface friction due to wind-stress, or the isopycnal or diapycnal mixing of water masses having different temperature/salinity properties. In this study, we argue that the main mechanism involved in the eddy generation can be determined from the knowledge of the temperature/salinity vertical structure in the eddies close to their generation site. Based on the complementary analysis of satellite and in-situ data in the tropical Atlantic Ocean, we show that 50% of the eddies do not present significant isopycnal temperature anomalies and are thus likely formed by frictional effects. The major part of these eddies do not participate to heat and salt transports. In contrast, the remaining 50% of eddies present significant isopycnal temperature anomalies and are likely formed by diapycnal mixing or advection of specific water-masses into a different background (through instability or other adiabatic processes). These eddies, that are mainly intensified in subsurface layers, likely conserve their initial anomalies and can transport heat and salt from their formation region.

1. Introduction

The Tropical Atlantic Ocean (TAO) is a key region for the inter-hemispheric exchange of heat, salt and mass by thermohaline circulation, large-scale currents and mesoscale eddies (e.g. Thomas and Zhai, 2013; Saenko et al., 2018). In the TAO, the upper ocean circulation is mainly composed of i) equatorial limbs of the North and South Atlantic anticyclonic subtropical gyres, ii) zonal equatorial currents and iii) near-coastal current systems (Fig. 1).

In the surface layer of the North and South Atlantic subtropical gyres, excess of evaporation over precipitation leads to the formation of relatively salty North and South Atlantic Waters (NAW and SAW, respectively; Fig. 1a) (Tsuchiya et al., 1992; Stramma and Schott; 1999; Bourlès et al., 1999a ; Stramma et al., 2005a-b). These water-masses have typical maximum salinities exceeding 37 in their formation region with densities of ~25.0 – 25.5 kg.m^{-3} (Bourlès et al., 1999a; Stramma and Schott, 1999; Kirchner et al. 2009). In contrast, in the surface layer of the equatorial Atlantic, the excess of precipitations associated with the atmospheric inter-tropical convergence zone leads to the formation of the relatively warm and fresh Tropical Surface Water (TSW; Fig. 1a) (e.g. Tsuchiya et al., 1992; Tomczak and Godfrey, 1994; Stramma et al., 2005b). With typical densities lower than 24.5 kg.m^{-3}, TSW extends within the mixed layer of the TAO (e.g. Stramma and Schott, 1999 ; Stramma et al., 2005a-b).

A fraction of NAW and SAW subducts from the mixed-layer into subsurface layers during winter to form North and South Atlantic Central Waters (NACW and SACW, respectively; Fig 1b) in the subtropical convergence zones around ±30-40° of latitude (e.g. Emery, 2003; Liu and Tanhua., 2019). This transport is mostly ensured by the large scale circulation forced by the Ekman wind-driven circulation that advects NACW and SACW equatorward along isopycnal surfaces in the main thermocline (~100-500 m) (e.g. Sprintall and Tomczak, 1993; Tomczak and Godfrey, 1994). The eastern part of these central water-masses can also be distinguished from their western part based on higher salinity especially in the northern TAO (e.g. Emery, 2003; Liu and Tanhua., 2019). These central water-masses, that are characterized by a linear temperature-salinity (Θ -S) relationship in the density range σ_θ ~ 25.8 - 27.1 kg.m^{-3}, are connected at around 15°N (Sverdrup et al. 1942; Emery and Meincke, 1986; Stramma and Schott, 1999; Stramma et al., 2005b). Another fraction of NAW and

SAW is advected west-equatorward by the North Equatorial Current (NEC) and the southern South Equatorial Current (sSEC), respectively (Fig. 1a). In the equatorial region these water-masses subduct and spread below the lighter TSW forming a subsurface salinity maximum in the upper thermocline, known as Subtropical Underwater (STUW; Fig 1b). STUW spreads within the density range $\sigma_\theta \sim 24.5\text{-}26.3$ kg.m^{-3} (Snowden and Molinari, 2003; Tsuchiya et al., 1992; Stramma and Schott, 1999; Stramma et al., 2005b). In the upper thermocline ($\sigma_\theta \sim 24$ - 24.5 kg.m^{-3}) of the eastern TAO, another subsurface salinity maximum water-mass is observed, but noticeably fresher than STUW (Wilson et al., 1994; Bourlès et al., 1999a; Urbano et al. 2008; Kirchner et al. 2009). This water-mass, known as East Atlantic Water (EAW, e.g. Bourlès et al., 1999a) is advected westward across the TAO by the northern SEC (nSEC; Fig 1b). In the western TAO, the observed subsurface salinity maximum in the upper-thermocline results from the advection, and mixing of the NAW, SAW and EAW by the complex circulation (Fig. 1a-b) (Bourlès et al. 2009a; Urbano et al., 2008; Kirchner et al. 2009). Below the base of the pycnocline ($\sigma_\theta > 26.0$ kg.m^{-3}), water-masses present Θ-S properties close to the Atlantic Subarctic Intermediate Water (ASIW) in the Northern TAO and Antarctic Intermediate Water (AAIW) in the Southern TAO (e.g. Emery, 2003).

Although the relatively complex large-scale circulation shown in Fig. 1 is important for the redistribution of water-masses, mesoscale eddies are also known to play a key role in the transfer and redistribution of energy, heat, salt and physical/biogeochemical properties from their generation regions to their dissipation sites (Chaigneau et al., 2011; Gaube et al., 2014; McGillicuddy 2016). These quasi-circular structures are ubiquitous in the TAO. They have typical radii of 30–100 km (Aguedjou et al., 2019) and can modulate ocean-atmosphere fluxes and thus the upper-ocean water-mass characteristics (Frenger et al., 2013; Villas Bôas et al., 2015; Renault et al., 2019; Seo et al., 2016; Foussard et al., 2019). They contribute to the mixing and redistribution of water-masses through several mechanisms such as eddy horizontal stirring, eddy-induced upwelling/downwelling, subduction or trapping and self-advection over long distances across the basin (McWilliams and Flierl, 1979; Herbette et al, 2004; Chelton et al., 2011), being able to connect eastern and western boundaries (e.g., Laxenaire et al., 2018). One final objective of this study is to determine which fraction of eddies could efficiently contribute to the potential transport and redistribution of heat and salt anomalies from their region of formation to their dissipation site. An important point, further discussed below, is that transport by eddies is mostly adiabatic and along isopycnal surfaces. Contrarily to what has been commonly done in previous studies, it is thus important to evaluate temperature and salinity anomalies associated with eddies along isopycnal surfaces instead of considering isobaric (or iso-depth) levels.

The vorticity of an eddy in geostrophic equilibrium is proportional to its isopycnal potential vorticity (PV) anomaly (Hoskins, 1985; Morel and McWilliams 1997; Herbette et al., 2003), which is a key quantity to analyze the formation and dynamics of eddies. PV is a conservative property for fluid particles in adiabatic evolution and many studies have shown how vortices can be formed by the displacement of particles in a background PV gradient. For instance, the formation of eddies by barotropic and/or baroclinic instabilities of mean currents is related to the existence of isopycnal PV gradient of opposite signs and can be interpreted as the result of the creation of opposite sign PV anomalies or dipolar vortical structures (Charney and Stern, 1962; Morel and McWilliams, 2001). Meridional advection on the planetary beta-plane (Wang, 2005), interaction of currents with seamounts, islands, or continental shelves (Aristégui et al., 1994; Herbette et al, 2004) can also be interpreted as creation of PV anomalies by adiabatic advection of particles. These processes are thought to play a significant role in the formation of mesoscale eddies at least in some regions of the TAO, east of the North Brazil Current (NBC) retroflection (e.g. Aguedjou et al., 2019). Some recent studies have shown that diabatic processes could also lead to the generation of PV anomalies and vortices. Indeed, theoretical and numerical studies have shown that diapycnal mixing (Haynes & McIntyre, 1987; Morel and McWilliams, 2001) and frictional effects, associated with lateral viscous layers (D'Asaro, 1988; Morel and McWilliams 2001; Akuetevi and Wirth, 2015), the wind (Thomas, 2005; Morel et al, 2006; Holmes et al, 2014; Holmes and Thomas, 2016) or with the bottom boundary layer (Benthuysen and Thomas, 2012; Gula et al, 2015 & 2016; Morvan et al, 2019), are all efficient mechanisms to modify PV and create vortical structures (Morel et al, 2019; Assene et al, 2020).

The origin of the processes (adiabatic, frictional or diapycnal mixing) involved in the generation of PV anomalies and vortices remains to be evaluated in nature. This is another key objective of the present study, which is very challenging, since the calculation of PV and its evolution require a three-dimensional description of currents and stratification. However, in the present study, we propose to derive qualitative information arguing that diapycnal mixing or isopycnal advection leads to PV anomalies with significant isopycnal *Θ/S* anomalies (e.g. Assene et al, 2020), in contrast to frictional effects which are expected to create PV anomalies but without significant isopycnal *Θ/S* anomalies.

In this study, we thus propose to combine in-situ *Θ/S* measurements with satellite altimetry data to estimate the isopycnal *Θ/S* anomalies of eddy cores at their generation sites in the TAO. In Section 2 we describe the datasets and methods used to characterize the *Θ/S* anomalies inside eddies. In Section 3 we first present the *Θ/S* characteristics of the large-scale water-masses over selected isopycnal levels. Second, we show case studies of *Θ/S* anomalies inside individual eddies to illustrate that *Θ/S* anomalies computed from isopycnal levels can strongly differ from the ones obtained along isobaric levels. Third, we characterize the *Θ/S* isopycnal structure of eddies in the entire TAO and focus in some particular areas of the northern TAO. These diagnostics help i) to estimate the fraction of eddies that can participate to the trapping and redistribution of heat and salt in the TAO and ii) to depict the mean isopycnal *Θ/S* anomalies in surface and subsurface intensified eddies. Finally, the possibility to infer where diapycnal mixing, isopycnal advection and/or frictional effects could play a significant role in their generation processes is discussed in Section 4 as well as the coherency of this information with the known dynamical features of the TAO.

2. Data and methods

2.1 Altimetry data and eddy tracking

Mesoscale eddies are identified and tracked in the TAO from daily maps of the Salto/Duacs Absolute Dynamic Topography (ADT) gridded product. This multimission satellite altimetry product, was optimally interpolated onto a 0.25°×0.25° longitude/latitude daily grid (Ducet et al., 2000; Le Traon et al., 1998; Duacs/AVISO+, 2018; Pujol et al., 2016) and is freely distributed by the Copernicus Marine Environment Monitoring Service (http://marine.copernicus.eu/).

Eddies were identified from January 2000 to December 2017, using the widely used algorithm developed by Chaigneau et al. (2008; 2009). An eddy is identified by its center, corresponding to a local extremum in Absolute Dynamic Topography (ADT), being maximum for anticyclonic eddies (AE) and minimum for cyclonic eddies (CE), and its external edge which corresponds to the outermost closed ADT contour around each detected eddy center. Eddy trajectories are constructed according to their polarity (cyclonic or anticyclonic) using the algorithm developed by Pegliasco et al. (2015). Briefly, this algorithm considers as part of the same trajectory, overlapping eddies with the same polarity detected at time *t* and *t + 1 day*. If several eddies overlap, a cost function is computed to determine the most similar eddy at the time *t + 1 day*. When no overlapping eddy is found neither at time *t + 1 day* nor *t + 2 days*, the trajectory is stopped and the eddy is considered as dissipated. As in Aguedjou et al. (2019), in order to consider only long-lived and coherent structures, we retained eddies lasting more than 30 days and having amplitudes and radii greater than 1 cm and 30 km, respectively. A total of ~7800 long-lived AE and ~8100 long-lived CE were detected in the TAO between 2000 and 2017. Readers interested in more detail regarding the main characteristics and seasonality of these eddies are invited to refer to Aguedjou et al. (2019).

2.2 Argo data

The vertical/isopycnal structure of mesoscale eddies is investigated using Θ/S profiles acquired by Argo floats in the TAO during the 2000-2017 period. These data were collected and made freely available by the Coriolis project and programs that contribute to it (http://www.coriolis.eu.org). Only profiles flagged as "good" were retained for our analysis. After an additional rigorous quality control (see supplementary material), retained vertical profiles were classified into three categories depending on whether Argo floats surfaced within AEs or CEs (detected from altimetry) or outside eddies. In our study we only considered Θ/S data between the surface ($\sigma_\theta < 23.5$ kg.m^{-3} in the TAO) and 1000 m depth ($\sigma_\theta \sim 27.5$ kg.m^{-3} in the TAO). In the TAO, a total of ~115000 Θ/S Argo profiles, representing ~80% of the initial dataset passed the quality control procedure, among which ~14500 (12.6%) surfaced within AEs and ~15300 (13.3 %) surfaced within CEs. Long-lived vortices detected by altimetry can thus be sampled several times by similar or different Argo floats at different phases of their evolution.

2.3 Isopycnal temperature anomalies at eddy generation sites

In order to investigate the isopycnal structure of eddies at their generation sites and estimate the mechanisms involved in their generation, depth-dependent *Θ/S* profiles were first projected onto density-coordinates (here density refers to potential density referenced to the sea-surface). Second, isopycnal temperature and salinity anomalies (*Θ'* and *S'*, respectively) were inferred for each profile by removing a local climatological profile representative of the large-scale background (e.g. Chaigneau et al., 2011; Pegliasco et al., 2015), also computed on density-coordinates. The local climatological profiles ($\bar{P}$) were obtained by weighted arithmetic means of all the available profiles (P_i) acquired outside eddies, within a radius of 200 km and separated by less than ±30 days (independently of the year) from the date of the considered profile (see supplementary materials). Third, we only retained profiles acquired in AEs or CEs close to their generation (within a radius of 200 km from their generation site identified from altimetry). Vortices were then further classified into three main categories, depending on whether isopycnal temperature anomalies were i) significant (positive or negative) in the surface layer, extending from the surface to the base of the pycnocline, ii) significant (positive or negative) in the subsurface layer below the base of the pycnocline, or iii) not significant neither above nor below the pycnocline (see supplementary materials). The corresponding eddies are then qualified as surface intensified, subsurface intensified or eddies with non-significant anomalies, respectively. Eddies having both surface and subsurface significant anomalies are considered as subsurface intensified.

In order to determine whether *Θ'/S'* are significant or not, an isopycnal temperature anomaly threshold was defined in a 1°x1° longitude/latitude grid at seasonal scale, from Argo profiles that surfaced outside eddies (see supplementary material). Fig. 2a-b show the annual mean of temperature anomaly thresholds for the surface and subsurface layers, respectively. In general, a given temperature anomaly profile is significant within the surface layer when the square root of its quadratic mean values (see Eq. E4 in supplementary material) integrated over the surface layer is greater than 0.2-0.5°C, except for some regions such as the frontal zone separating NAW from TSW, where *Θ'* threshold reaches up to 0.8°C (Fig. 2a). In contrast, threshold values of *Θ'* within the subsurface layer are much lower and on average less than 0.3°C. However, around the frontal zone along which the NEC is flowing, high threshold values are still noticed reaching up to 0.8°C (Fig. 2b). For a given density, *Θ'* and *S'* are proportional and of the same sign, so that isopycnal maps of *Θ'* or *S'* are similar by definition. We thus hereinafter only focus on *Θ'* along isopycnal levels.

3. Results

3.1 Large-scale distribution of isopycnal temperature in the TAO

In order to better understand the eddy signature on *Θ* along isopycnal surfaces, we first briefly depict the large-scale water-mass temperature distribution in the TAO along two isopycnal levels. As such, Fig. 3 presents the mean *Θ* on σ_θ = 25.5 kg.m^{-3} and σ_θ = 27.2 kg.m^{-3} levels, obtained from Argo floats that surfaced outside eddies. On the shallower/lighter density-level, we can observe the noticeable warmer areas located within the subtropical gyres where NAW and SAW are located (Fig. 3a,d). On σ_θ = 25.5 kg.m^{-3}, these water-masses have typical temperatures of 24°C and 22.5°C, respectively (Fig. 3a,d). The along-isopycnal *Θ* decreases equatorward from the gyre centers. In the eastern TAO, where EAW is originated, *Θ* decreases to ~20°C and S is lower than 36 (see also on Fig. 3d). Along the equator a relative warm core (*Θ* ~ 22°C) water-mass is advected eastward by the EUC (see Fig. 1 and Fig. 3a). The temperature of this water-mass, also characterized by relatively high salinities (not shown but see, e.g. Hormann and Brandt, 2007; Kolodziejczyk et al., 2009 Da-Allada et al., 2017), slightly decreases eastward. Finally, in the eastern boundary upwelling systems (Canary and Benguela), the mean *Θ* is lower than 18°C on σ_θ = 25.5 kg.m^{-3} due to the presence of the wind-forced coastal upwelling (Fig. 3a). The σ_θ = 25.5 kg.m^{-3} isopycnal layer deepens from ~40 m in the eastern TAO to ~140 m in the western TAO at latitudes of ±20° (black lines in Fig. 3a). The westward deepening of this isopycnal layer, which is associated with the lower part of the thermocline/pycnocline, is reduced along the equator where its depth varies from 50 m in the Gulf of Guinea to ~100 m off Brazil.

On the σ_θ =25.5 kg.m^{-3} (σ_θ =27.2 kg.m^{-3}, respectively) density layer, *Θ* distribution shows a strong isopycnal *Θ* front that separates the warmer and saltier NAW (NACW) from the colder and fresher EAW (SACW) and extends across the basin. East of ~30°W, this front is known as the Cape Verde Frontal Zone (CVFZ) (Zenk et al; 1990; Pérez-Rodriguez and Marrero-Diaz, 2001; Martínez-Marrero et al., 2008; Tiedemann et al., 2018), which is an active area of water-mass exchange associated with the formation of mesoscale eddies (e.g. Dadou et al., 1996; Schütte et al., 2016). However, we hereafter simply refer to the frontal zone to indicate the connection area between NACW and SACW. The NEC flows along this frontal zone, which is oriented southwestward from 20°N in the eastern TAO to 10°N in the western TAO (see also Fig. 1). This front is clearly visible down to σ_θ = 27.2 kg.m^{-3} (Fig. 3b) where it is more diffuse and the strongest Θ gradients are observed southward, between 10°N and the equator. At this density level, the frontal zone is much more zonal, and NACW and SACW have typical temperatures of 10-11°C and 5-6°C, respectively (Fig. 3b,d). The mean depth of this isopycnal level is of ~650 m in a large part of the TAO (black lines in Fig. 3b), and deepens to 750-900 m poleward of latitudes ±20°.

Figure 3c presents the meridional Θ section at 35°W. Warmer waters with Θ greater than 20°C are located above the σ_θ = 26.0 kg.m^{-3} isopycnal layer and are associated with the previously described NAW, SAW and TSW. TSW is the warmest water-mass, with Θ reaching 28°C around the equator, but exhibits the lowest surface salinity of 35.5-36 (not shown) due to the excess of precipitation to evaporation in this area. Below the σ_θ = 26.0 kg.m^{-3} density layer, are located the distinguishable warmer NACW and cooler SACW, separated by the Θ front that becomes more diffuse below σ_θ = 27.0 kg.m^{-3}.

Θ/S diagrams and the main water-mass characteristics found in the TAO are depicted in Figure 3d. They were constructed from Argo float that surfaced outside eddies within the northern, southern and eastern parts of the TAO (see boxes delimited in magenta in Fig 3.a). This Figure confirms that TSW is much fresher and lighter than NAW or SAW and that NACW is warmer and saltier than SACW along isopycnal levels.

3.2 Case studies of iso-depth versus isopycnal temperature anomalies in mesoscale eddies

Estimates of Θ and *S* anomalies within an eddy can strongly differ whether we use a depth-coordinate system or a density-coordinate system. In order to better familiarize the reader with this concept, and to help the interpretation of the results described in the following Sections, we here describe temperature anomalies observed in three individual mesoscale anticyclonic eddies at their generation sites, using both the depth- and density-coordinate systems. These three eddies (AE1, AE2 and AE3, respectively), detected by their ADT signature, were sampled by Argo floats in the western (AE1, Fig. 4a), central (AE2, Fig. 4b) and eastern parts

(AE3, Fig. 4c) of the northern TAO. Their centers are approximately located at (55°W;15°N), (32°W-19°N) and (22°W-10°N), respectively. They have typical amplitudes of 3.3 cm, 4.2 cm, and 1.7 cm, and associated radii of ~100 km, ~70 km and ~80 km, respectively. Their eddy kinetic energy was relatively similar, varying between 85 and 100 $cm^2 s^{-2}$, a typical range for the northern TAO (Aguedjou et al., 2019), and their mean vorticity was of 4.3 $x10^{-5}$ s^{-1}, 5.1 $x10^{-5}$ $s^{-}1$ and 2.2 $x10^{-5}$ s^{-1} respectively.

Although the 3 eddies were sampled by Argo floats within their core, AE1 and AE2 were sampled relatively close to their edge (Fig. 4a-b), whereas A3 was sampled in the vicinity of its eddy center (Fig. 4c). Temperature anomalies observed using a depth-coordinate system are positive for the 3 case-study eddies (Fig. 4d-f, magenta lines), as expected for AEs, except for A2 whose anomaly is slightly negative below 200 m. Indeed, in depth-coordinates, due to the isopycnal depression (heaving, respectively) occurring inside surface-intensified AEs (CEs), they induce positive (negative) anomalies (e.g. Assassi et al., 2016; Keppler et al., 2018). AE1, has a maximum temperature anomaly of 3.5°C centered at 400 m depth and is likely a subsurface intensified eddy with a core extending from 100 m to 600 m depth (Fig. 4d). When eddy temperature anomalies are first computed in density-coordinates and then re-projected on depth-levels, the maximum Θ' is of ~1°C and rather observed along σ_θ ~ 27.1 – 27.2 kg.m^{-3} isopycnal levels located between 400 and 600 m depth (Fig. 4d, red line) thus confirming that A1 is subsurface-intensified. Fig. 4g compares the Θ/S diagrams for the Argo profile acquired inside the vortex (red) and the corresponding climatological profile obtained from profiles outside eddies (green). It can be misleading since there exists strong discrepancies between both profiles in low density ranges (σ_θ = 24.0-25.5 kg.m^{-3}) (Fig. 4d). However, given the curvatures of isopycnal lines and of the vertical profiles, the strongest isopycnal eddy Θ/S anomalies are obtained in the subsurface layer containing NACW. Thus, for this particular AE1 case-study, temperature anomalies are located in subsurface and of the same sign (positive) for both coordinate systems.

In AE2, temperature anomalies computed in depth-coordinates are positive between the surface and 250 m depth, and slightly negative below 250 m (magenta line in Fig. 4e). The maximum anomaly is of ~1.5°C at ~150 m depth, thus AE2 is likely surface intensified. However, when computing Θ' in density-coordinates, AE2 is characterized by negative Θ' in the surface layers reaching maximum negative anomalies of -1.5°C at ~170 m depth (red line in Fig. 4e). In fact, the vertical displacement of isopycnal surfaces associated with vortices in geostrophic balance explains most of the anomalies in depth-coordinates (e.g. Assassi et al., 2016; Keppler et al., 2018). As a consequence, the downwelling of isopycnal surfaces in surface intensified AEs, results in positive temperature anomalies in depth-coordinates, as observed in Fig. 4e. In contrast, isopycnal anomalies are observed only if eddies contain water from a remote region having distinct Θ-S characteristics, or if diapycnal mixing locally modifies the thermohaline structure of the water column. In AE2, maximum negative isopycnal anomalies were observed in the surface layer containing NAW (Fig. 4h). AE2 is thus a striking example of differences that can exist when computing anomalies using depth versus density-coordinates. These discrepancies are problematic in particular for the estimates of anomalous heat or salt eddy contents, and their associated transport, which are generally computed in depth-coordinates instead of isopycnal-coordinates.

In AE3, significant positive temperature anomalies computed from depth-coordinates are observed from the surface to 200 m depth (Fig 4f). Maximum anomalies of ~3.5°C are observed at ~50 m depth, revealing that AE3 is a surface-intensified AE using depth-coordinates. However, isopycnal Θ' anomalies, re-projected on depths, show that this eddy does not contain significant water-mass anomalies relative to the background large-scale environment (Fig. 4f). The isopycnal Θ-S structure within the eddy is similar to the one usually observed in this region, with EAW and SACW in the surface and subsurface layers, respectively (Fig. 4i).

To summarize, based on 3 case-study AEs, we have shown that isopycnal Θ' anomalies can strongly differ from anomalies computed from the more commonly used depth-coordinate system. Obviously, similar conclusions hold for CEs that generally depict negative anomalies in depth-coordinate system, but that can show positive, negative or null anomalies in density-coordinate system. Significant eddy anomalies along isopycnal levels are associated to isopycnal advection from remote regions or diapycnal mixing.

3.3 Spatial distribution of isopycnal temperature anomalies in TAO new-born eddies

Figure 5 shows the spatial distribution of surface-intensified, subsurface-intensified eddies and eddies with negligible anomalies at their generation sites in the TAO. A first striking result is that about half of the analyzed new-born AEs and CEs have a weak and non-significant isopycnal Θ' relatively to their local environment close to their generation site. They cover all areas and their spatial distribution is quite identical for AEs and CEs (Fig. 5e-f and Table 1).

Thus, about half of the analyzed new-born AEs (52%) and CEs (50%) have a significant Θ' anomaly at their generation sites. Among AEs (CEs, respectively) having significant anomalies, ~25% (27%) are only surface-intensified whereas ~75% (~73%) exhibit maximum isopycnal anomalies at subsurface (Table 1). Note however, that vortices with subsurface anomalies can also sometimes have significant surface anomalies. This category of eddies represents ~34% (~32%) of subsurface-intensified AEs (CEs). The spatial distribution of AEs and CEs having significant isopycnal Θ' is almost similar in surface and subsurface layers (Fig. 5a-b and 5c-d). About 57% (~53%) of surface (subsurface) intensified eddies are characterized by positive Θ' (Fig. 5 and Table 1). However, within the surface layer of the Southern Hemisphere, more than 82% (55%, respectively) of AE (CE) with significant anomalies have positive (negative) Θ'. In this region of the TAO, eddies with significant Θ' are less numerous and their maximum isopycnal Θ' (±0.3°C) are observed around the Benguela upwelling system. In contrast, in the Northern Hemisphere, positive and negative Θ' are more similarly distributed with magnitude reaching up to ±0.8°C along the frontal zone (Fig. 5a-b). Within the subsurface layer, ~56% (65%, respectively) of the significant AEs (CEs) in the Northern Hemisphere have a negative (positive) Θ' versus ~38% (44%) of AEs (CEs) in the Southern Hemisphere (Fig. 5c-d and Table 1). Again, the dominance of relatively cold AEs and warm CEs in subsurface may seem unusual for those who are used to work in depth-coordinates where the sign of the anomalies are largely driven by the deepening/heaving of isopycnal layers (see Section 3.2). Moreover, strong anomalies of ±0.4°C are observed within the frontal zone separating SACW and NACW (Fig. 5c,d). As shown in Fig.2, this area is characterized by a high value of the temperature threshold highlighting the strong spatio-temporal temperature variability of this frontal zone.

3.4 Eddy isopycnal structures in selected TAO regions

Three sub-regions (R1 to R3, see Fig. 2-5) were defined according to their large-scale dynamics and characteristics (Fig.1, Fig. 2 and Fig. 3a-b). R1 extends along the frontal zone separating NACW from SACW (Fig 2). The westward NEC which flows along the frontal zone is mainly fed by the eastern branch of the North

Atlantic subtropical gyre but also by the northern branch of the Guinean Dome (Fig. 1). Further west, a part of the NEC retroflects cyclonically and feeds both the eastward North Equatorial Counter Current (NECC) and the eastward North Equatorial Undercurrent (NEUC) (Fig. 1a-b; e.g. Stramma and Schott, 1999; Bourlès et al. 1999a; Schott et al., 2004). The large-scale isopycnal temperature distribution (Fig. 3) shows that the NEC flows along the frontal zone that separates relatively warm and salty waters of the North Atlantic subtropical gyre from cooler and fresher waters of the equatorial Atlantic Ocean (Fig. 3). This frontal zone is known to exhibit strong meanderings and eddy generations (e.g. Dadou et al., 1996; Shütte et al., 2016; Aguedjou et al., 2019). In R2, that extends from north-east Brazil to west Africa between 0°N and 10°N (Fig. 5), is found the zonal equatorial dynamics (Fig. 1). In this region, strong instabilities are frequently observed, in particular due to the horizontal shear between the nSEC and NECC (Fig. 1) (e.g. Weisberg and Weingartner, 1988; Kelly et al., 1995; Athié and Marin, 2008; Von Schuckmann et al., 2008, Aguedjou et al., 2019). Finally, the subregion R3 includes the NBC retroflection (Fig. 1a-b), and is populated by relatively large and energetic eddies whose surface properties (size, amplitude, eddy kinetic energy) exhibit a strong seasonal variability (e.g. Aguedjou et al., 2019).

Figure 6 shows for these 3 subregions the mean vertical Θ' profiles inside AEs and CEs at their generation sites, using density-coordinates. As already discussed, the 3 sub-regions show a high number of non-significant anomaly profiles representing 40% to 60% of observed eddies (Fig. 6, in black).

In R1, between 75% (72%) of the new-born AEs (CEs) sampled by Argo floats and that have a significant temperature anomaly, are subsurface intensified (Fig. 6a,d). Surface AEs (solid lines in Fig. 6a) and CEs (solid lines in Fig. 6d) are characterized by average temperature anomalies of ±0.5-0.7°C between $\sigma_\theta \sim 25.5$ and 26.0 kg.m^{-3}. Subsurface AEs (dotted lines in Fig. 6a) and CEs (dotted lines in Fig. 6d) show maximum anomalies of ±0.4°C between $\sigma_\theta \sim 27$ kg.m^{-3} and $\sigma_\theta \sim 27.2$ kg.m^{-3} except subsurface cold CEs whose mean anomaly of -0.5°C is found between $\sigma_\theta \sim 26$-26.5 kg.m^{-3}. Interestingly, around 73% (65%, respectively) of these subsurface eddies are cold (warm) for AEs (CEs).

In R2, similarly to what is observed in R1, 65% of the CEs and ~70% of the AEs that present a significant Θ' are of subsurface (Fig. 6b,e). Around 82% (65%, respectively) of the subsurface sampled AEs

(CEs) have cold (warm) anomalies and their maximum anomalies of ±0.3-0.4°C are located at $\sigma_\theta \sim 27.2$ kg.m^{-3} (Fig. 6b,e). The remaining surface-intensified eddies have anomalies of ±0.5°C, with the maximum located in the density range of the eastward NECC and the westward nSEC, which carry relatively warm and cold water, respectively (Fig. 1a & 3a).

In R3 (Fig. 6c,f), unlike in the two previous areas, very few new-born eddies were sampled by Argo floats. Moreover ~55% of the AEs and ~65% of the CEs sampled at their generation sites do not exhibit significant temperature anomalies. The remaining sampled new-born eddies are characterized by relatively large anomalies, reaching ±1°C for CEs and ~ ±0.7°C for AEs. Note, that the relatively small number of sampled eddies is due both to the very few number of Argo floats in R3 and to the reduced size of this area. AEs characterized by positive *Θ'* (red lines in Fig. 6c) show anomalies of ~0.5°C, observed at $\sigma_\theta = 26$ kg.m^{-3} for surface AEs, and $\sigma_\theta = 26.8$ kg.m^{-3} for subsurface AEs. Surface intensified CEs predominantly show strong positive and negative anomalies that are maximum at $\sigma_\theta = 25.5$ kg.m^{-3} (solid lines in Fig 6f). In contrast, subsurface CEs mainly show positive temperature anomalies of 0.5°C at the base of the thermocline or at $\sigma_\theta \sim 27$ kg.m^{-3} (dotted lines in Fig. 6f). Note that the 3 profiles classified as cold subsurface CEs (blue dotted line in Fig. 6e) are characterized by strong positive anomalies between $\sigma_\theta = 24.5$ kg.m^{-3} and $\sigma_\theta = 26.7$ kg.m^{-3} and weak negative anomalies in deeper levels. Integrated in the water column, these deeper negative anomalies, that occupy a thicker layer, prevail and lead to a negative heat content anomaly that explains the classification of these profiles as "cold subsurface CEs. In R3, the sampled new-born eddies were mainly formed on the eastern flank of the NBC retroflection (not shown), where relatively strong temperature gradients exist. In the subsurface layer, isopycnal mixing of NACW and SACW takes place (eg. Kirchner et al., 2009).

4. Qualitative analysis and discussion

4.1 Eddy vertical structure and potential implications for heat and salt transports

The first striking result of our analysis, underlined in Fig. 5, is that about half of the analyzed eddies have non-significant isopycnal *Θ'/S'* at their generation site. Among the other half of the eddies, characterized by significant isopycnal *Θ'/S'*, more than 70% are subsurface-intensified, with maximum anomalies below the pycnocline. Within these eddies, the strongest temperature anomalies, averaged within the surface (subsurface, respectively) layer, are of ±1.2°C (±0.8°C). These maximum anomalies are found in the Northern Hemisphere, especially within the frontal zone separating the NACW and SACW, and along which the NEC flows westward across the TAO (Fig. 5). In the Southern Hemisphere, averaged isopycnal *Θ'/S'* anomalies in the surface/subsurface layers are generally weaker, except in the Benguela upwelling system where the anomalies are as high as in the Northern Hemisphere. The high number of subsurface intensified eddies obtained in our study have been also previously reported in different areas of the TAO, from both numerical simulations and in-situ data. For instance, in the Canary and Benguela upwelling systems, Pegliasco et al. (2015) estimated that subsurface-intensified eddies represent between 40 and 60% of the total number of eddies. Although their analysis was based on depth-coordinates and did not specifically focused on new-born eddies, these authors also showed that 40-60% of the sampled eddies do not have statistically significant *Θ'/S'*, in agreement with our results. Other studies also revealed the presence and persistence of subsurface-intensified structures in various parts of the Atlantic Ocean, from eastern to western boundary currents regions and from the north to the south Atlantic subtropical gyres (e.g. Schutte et al., 2016; Garraffo et al., 2003; Assene et al., 2020; Amores et al., 2017; Laxenaire et al., 2020). However, as already discussed by Pegliasco et al. (2015), the high number of subsurface eddies could be influenced by a slight sampling bias in the Argo data. Indeed, Argo floats drift for 10 days at a nominal parking depth of 500-1000 m and may therefore be preferentially trapped within subsurface eddies that reach these depths.

In terms of tracer transport, our results would suggest that only half of the analyzed eddies (eddies with significant anomalies) might potentially contribute to the heat and salt transport within the basin. However, the efficiency of the eddies to redistribute heat and salt from their formation region strongly depends on the ambient *Θ/S* characteristics at their dissipation sites and whether or not the transported water-masses exhibit similar properties than the ambient ones. Thus, in order to estimate whether the sampled mesoscale eddies significantly contribute to the *Θ/S* transport and redistribution in the TAO, we computed the temperature anomalies that these eddies would create at their dissipation site if they advected isopycnally, and without any mixing or modification, the water-mass properties from their region of formation. First, for each sampled eddy, isopycnal

Θ' was estimated by removing the mean climatological isopycnal Θ profile at its dissipation site (which corresponds to the last position of the altimeter-derived eddy trajectory) from the isopycnal Θ profile inside the eddy at its birth location. Second, the obtained Θ' profile where compared to the temperature threshold (e.g. Figure 2) at the dissipation site to determine whether Θ' are significant, and the eddy contribute to the heat and salt transport, or not. Applying this methodology, we show that more than 80% of eddies that are formed in the TAO with non-significant Θ' remain non-significant when they dissipate and do not participate to the heat and salt transport. The remaining ~ 20% of eddies whose anomalies become significant, and therefore may modify their environment, are distributed throughout the basin without any particular spatial structuring. In contrast, ~80% of subsurface-intensified eddies (independently of warm and cold) at their generation sites are characterized by significant anomalies when they dissipate, suggesting that these eddies play a key role in the heat and salt transports. This fraction is somewhat reduced to 60-65% for surface-intensified eddies. To conclude, these estimates suggest that ~20% of the non-significant and ~80% of the significant new-born eddies, thus representing ~50% of the total sampled eddy population, can significantly impact heat and salt redistributions. It is important to recall that Θ/S anomalies computed in depth-coordinates are largely influenced by the vertical displacement of isopycnal layers and do not reflect the eddy heat and salt contents that participate to the redistribution of tracers. As such, isopycnal coordinates must be considered when evaluating heat/salt transport by eddies.

4.2 Vorticity, PV anomalies and diabatic effects

The vorticity of an eddy is related to its PV anomaly which, as mentioned in Section 1, is determined by diapycnal mixing, frictional effects and adiabatic isopycnal advection of water-masses by large scale currents. Large-scale isopycnal advection and diapycnal mixing lead to the creation of both isopycnal Θ/S and PV anomalies. Conversely, frictional effects, here associated with wind-stress because bottom and lateral frictions play little role in the offshore TAO, modify the PV and contribute to the formation of eddies but with only weak and non-significant tracer anomalies. Vortices whose PV is shaped by diapycnal mixing or isopycnal advection by large scale currents are thus expected to be associated with specific Θ/S and PV anomalies. In order to better understand this process and interpret the significant *Θ/S* anomalies observed in the TAO eddies, we computed a mean large-scale rescaled PV (see Morel et al., 2019; Asséné et al., 2020; Delpech et al., 2020) as:

$$PV = -\left(\vec{\nabla} U + \vec{f}\right).\vec{\nabla} Z(\rho)$$

where U is the geostrophic velocity field computed from the World Ocean Atlas *Θ/S* climatology (Locarnini et al., 2018; Zweng et al., 2018) with a level of no motion at 1000 m depth, *f* is the Earth rotation vector , whose projection on the local vertical axis defines the Coriolis parameter f, and Z(ρ) is the depth as a function of the potential density. The rescaled PV is close to the quasi-geostrophic PV and it scales as a vorticity with a reference value at rest close to f (see Morel et al., 2019; Asséné et al., 2020; Delpech et al., 2020). It also has the same properties as the traditional Ertel PV but for this traditional form, vertical sections are dominated by the signature of the pycnocline, and the dynamical signal associated with isopycnal variations of PV is difficult to identify. This difficulty is overcome by choosing Z (ρ*) = z for a specific location, where the density profile ρ*(z) is typical of the stratification of the area and can be taken as a reference to rescale PV. This methodology was applied by Assene et al. (2020) and following them, we choose our reference profile at 27°W – 7.5°N, a dynamically less intense area corresponding also to a lower surface density. Figure 7a,c shows the distribution of the obtained rescaled PV, averaged within both a near-surface (σ_θ =25.75 - 26.5 kg.m^{-3}) and a subsurface layer (σ_θ =26.9 - 27.4 kg.m^{-3}). Superimposed to the PV distributions, are also shown the mean *Θ* contours averaged within the same layers (Fig. 7a,c). In R1, a reservoir of relatively strong (weak, respectively) positive PV, associated with relatively cold (warm) water is observed on the southern (northern) edge of the thermal front in the surface layer (Fig. 7a). Thus in this layer, an isopycnal PV advection tends to generate either i) positive PV anomalies associated with negative *Θ'*, leading to the formation of cold core surface CEs, or ii) negative PV anomalies associated with positive *Θ'*, leading to the generation of warm-core surface AEs. This PV-*Θ* relationship is better depicted in Fig. 7b. In contrast, in R2, maximum positive PV are associated with warmer *Θ*, suggesting that isopycnal advection tends to generate cold AEs and warm CEs in the surface layer of this region (Fig. 7a-b). In R3, as shown in Fig. 7b, the PV-*Θ* relationship is more complex and not strictly monotonic, suggesting that both warm and cold CEs and AEs can be generated by isopycnal advection, although the general tendency is closer to the R2 region (cold AEs and warm CEs). From Figure 6, we effectively observed a higher number of cold AEs in the surface layer in R2 and R3, representing ~ 66% of the significant surface-intensified eddies. Note, that in the very dynamic surface layer, which is in constant interaction with the atmosphere, other processes can modify the isopycnal Θ/S and PV structures, such as wind-stress, diapycnal mixing, or outcropping of isopycnal layers.

PV-Θ relationships were also examined in the subsurface layer where we note a general northward increase of both the PV and Θ (Fig. 7c). This distribution, as well as the main PV-Θ relationship shown in Fig. 7d, suggests that large-scale isopycnal advection leads to the formation of cold subsurface AEs and warm subsurface in the TAO. Thus, isopycnal advection likely explains the dominance (65-80% of the subsurface structures) of warm CEs and cold AEs observed from the Argo profiles in R1 and R2 (Fig. 6). To conclude, the most likely mechanism for the generation of PV anomalies of eddies without isopycnal Θ'/S' signature is friction. Likewise, friction probably also plays a major role in the generation of PV anomalies for vortices exhibiting significant but unstructured Θ'/S' signature. Note that even a constant wind (with weak Ekman pumping effects) is able to modify PV along a front (Thomas, 2005), a process that has been shown to lead to the destabilization of upwelling currents (Morel et al., 2006), strong modification of Ekman drift (Morel and Thomas, 2009) or the reinforcement of preexisting vortical structures (Holmes et al., 2014).

4.3 Limitations of the study

Diagnostics proposed in this study remain mostly qualitative, but, to our knowledge, it is the first attempt to determine the importance of diabatic effects in the generation of eddies and their associated Θ/S and PV properties from observations. The respective influence of the wind-stress and diapycnal mixing in the formation of surface and subsurface vortices can serve as reference for realistic numerical models, for which diabatic processes are parameterized. Given the reasonable number of eddies sampled in this study, the statistics calculated here are thought to be significant, but could obviously be refined in the future, when more observations become available.

Although our classification of significant versus non-significant Θ'/S' is robust, it is important to point out some limitations of our diagnostics. First, the fact that eddies must be sampled at their generation (±200 km) sites strongly reduces the number of analyzed eddies. Second, some of Argo profiles classified as outside eddy profiles might have sampled vortices which were not detectable by altimetry, such as within the NBC retroflection or the eastern equatorial Atlantic where numerous subsurface eddies were numerically identified with no surface signal (Garraffo et 2003, Asséné et al., 2020). The isopycnal *Θ* climatology, obtained from profiles supposedly acquired outside eddies and used to evaluate eddy anomalies could be slightly spoiled by this effect. However, given the very large number of Argo profiles available, we believe this remains marginal. Likewise, some regions such as equatorial areas, the Gulf of Guinea or the central part of the Southern Hemisphere are characterized by a few number of detected eddies (see Aguedjou et al., 2019). This compromises the evaluation of robust statistics in such regions. Third, the exact location, relative to the eddy-centers, of Argo floats that surfaced within eddies were not considered when calculating the eddy *Θ'/S'*. However, both theoretically and practically, Argo vertical profiles are on average acquired at a distance of 2/3 the eddy radius from the eddy center (e.g. Chaigneau and Pizarro, 2005; Pegliasco et al., 2015). The mean distribution of Argo floats suggests that *Θ'/S'* obtained in our study are more likely representative of the outer eddy structure than the eddy center. Although it may slightly impact our results, eddy cores can generally be considered as homogeneous in *Θ/S* and the general discussion on the mechanisms involved in the generation of *Θ/S*, that shape the whole eddy structure from the eddy center to the eddy edge, remains valid.

5. Summary and perspectives

Combining 18 years of satellite altimetry and *Θ/S* data acquired by Argo floats in the TAO, we first showed that isopycnal *Θ/S* anomalies can strongly differ from the ones obtained using depth-coordinates. Indeed, although AE (CE, respectively) mostly induced positive (negative) *Θ/S* anomalies in depth-coordinates, both AE and CE can exhibit positive, negative or non-significant isopycnal *Θ/S* anomalies. In fact, *Θ/S* anomalies in depth-coordinates are largely influenced by the vertical displacement of isopycnal layers (see also Keppler et al., 2018) and do not reflect the heat and salt contents of the eddies that participate to the net transport of tracers in the ocean. We then focused on the vertical structure of eddies close to their generation site, and investigated the proportion and distribution of eddies having significant and non-significant isopycnal temperature anomalies. Our results show that more than half of the total analyzed new-born eddies in the TAO are characterized by non-significant *Θ'*, underlining the effect of the wind-stress in their generation. In contrast, the second half, composed of 70% of subsurface-intensified eddies, having their maximum anomalies below the pycnocline, and of 30% of near surface-intensified eddies, are likely formed by mixing and/or lateral advection. As a consequence, in terms of tracer transport, our results would suggest that eddies that are generated with a significant Θ'/S' mostly contribute to heat and salt transport in the TAO. Indeed ~80% of subsurface-intensified and ~ 65% of surface-intensified eddies remained with a significant Θ'/S' at their dissipation regions. Thus, they can potentially modify the Θ/S properties of their environment when the water initially trapped in their cores is released. In contrast, among eddies that are generated with non-significant Θ'/S', only 20% have shown a significant anomaly at their dissipation sites. Refined diagnostics in three selected subregions in the northern TAO, were proposed. Along the frontal zone and in the northern equatorial subregions, the mean vertical structure of eddies is dominated by the subsurface-intensified eddies (65-75%) with maximum anomalies reaching up to ±0.5 °C mostly found between σ_θ = 27 and 27.2 kg.m^{-3} isopycnal layers. Strikingly, for these subsurface-intensified eddies, ~73% of AEs exhibit a negative maximum anomaly whereas ~65% of CEs maximum anomalies are positive. In the third subregion, within the NBC retroflection, results are questionable because of the reduced number of eddies sampled by Argo profiles at their generation sites.

The potential links between Θ'/S' and adiabatic or diabatic generation of PV anomalies were also discussed in each subregion. For eddies with significant anomalies intensified in the surface layer, PV-Θ relationships suggest that isopycnal water-mass advection mostly explains the generation of cold core AEs observed in R2 and R3 areas. In contrast, in R1 isopycnal advection would preferentially lead to the generation of cold (warm, respectively) core CEs (AEs). Observations show no preference in Θ'/S' anomalies, suggesting that other processes such as wind-stress, diapycnal mixing, or outcropping of isopycnal layers are likely to modify the Θ'/S' and PV structure of water-masses. In the subsurface-layer, water-mass advection is also suggested to explain the formation of warm (cold, respectively) core CEs (AEs) especially in R1 and R2, which indeed corresponds to the distribution dominantly observed.

Our analysis remains qualitative, but an important result is that the wind-stress is a major source for the generation of PV anomalies and vortices in the TAO given the fraction of eddies formed with non-significant Θ'.

This is coherent with recent numerical studies invoking the strong influence of the wind-stress on the generation or reinforcement of vortices (Thomas, 2005; Morel et al, 2006; Holmes et al, 2014; Holmes and Thomas, 2016). It is the first time that such a diagnostic has been obtained from observations. Note that numerical results have also revealed a strong influence of bottom friction (Benthuysen and Thomas, 2012; Gula et al, 2015, 2016; Morvan et al, 2019), but this seems very challenging to confirm with observations since it is difficult to identify Argo profiles associated with newly born deep subsurface vortices, as the latter generally have weak SSH signature.

As far as perspectives are concerned, this study proposed new diagnostics (Fig. 6) that can be useful for numerical models. As mentioned above, diabatic processes are parameterized in the models, and thus imperfectly represented. We here argue that it cannot only be problematic for the representation of the water-mass characteristics, but it also strongly influences the PV and vorticity structure of generated eddies. Combined diagnostics involving isopycnal Θ'/S' and vorticity of eddies is thus challenging for numerical results. In particular, since a major fraction of the observed eddies are associated with non-significant Θ/S anomalies, frictional effects are thought to play a major role in the generation of their PV structure. Parameterizations of frictional effects are very difficult to evaluate and remain one of the Achille's heel of circulation models at mesoscale. The proposed diagnostics can thus be very useful to compare different parameterizations. Further diagnostics based on observations are possible too. First, it would be interesting to combine isopycnal Θ/S structures with trajectories to infer the transport of water-masses from a region to another. It would also be informative to study the long term behavior of specific long-lived eddies, having been sampled at different times by Argo floats, to analyze the evolution of their heat/salt contents. Applying the present general approach to other regions is of course interesting too. In particular, in the energetic area such as the Gulf Stream and Kuroshio or in specific region where wind-stress curl lead to the eddy generation (Canaries, Ierapetra, etc.). Finally, when a significant number of Argo floats will be equipped with biogeochemical sensors (dissolved oxygen, nutrients, chlorophyll-a, pH, …), it will be very interesting to evaluate if there exists some structuring in the transport of biogeochemical tracers by AEs and CEs, in particular in the TAO.

Acknowledgments:

This work was supported by the Alti-ETAO project founded by the French National Center for Space Studies (CNES) through the Ocean Surface Topography Science Team (OSTST) and supported by the French National Institute of Sciences of the Universe (INSU/CNRS). This work is also a contribution to the junior team “SAFUME” (JEAI-SAFUME) associated with the French National Research Institute for Development (IRD) and to the EU H2020 TRIATLAS project under grant agreement 817578. M. Aguedjou was supported by a PhD fellowship from the IRD and the Cultural Action and Cooperation Service (SCAC) of the French Embassy in Benin.

Gridded altimetry data were produced by SSALTO/DUACS and distributed by the Copernicus Marine Environment Monitoring Service (http://marine.copernicus.eu/) and Argo data were collected and made freely available by the Coriolis project and programs that contribute to it (http://www.coriolis.eu.org).

References

Aguedjou, H. M. A., Dadou, I., Chaigneau, A., Morel, Y., & Alory, G. (2019). Eddies in the Tropical Atlantic Ocean and their seasonal variability. Geophysical Research Letters, 46. https://doi.org/10.1029/2019GL083925

Akuetevi, C. Q. C. and Wirth, A. (2015). Dynamics of turbulent western-boundary currents at low latitude in a shallow-water model, Ocean Sci., 11, 471–481, https://doi.org/10.5194/os-11-471-2015.

Amores, A., Melnichenko, O. and Maximenko, N. (2017), Coherent mesoscale eddies in the North Atlantic subtropical gyre: 3-D structure and transport with application to the salinity maximum, *Journal of Geophysical Research: Oceans*, *122*(1), 23–41, doi:10.1002/2016jc012256.

Aristégui, J., Sangra, P., Hernandez-Leon, S., Canton, M., Hernandez-Guerra, A., & Kerling, J. L. (1994). Island-induced eddies in the Canary Islands. Deep-Sea Research Part I: Oceanographic Research Papers, 41(10), 1509–1525. https://doi.org/10.1016/09670637 (94) 90058-2

Assasi, C., Morel, Y., Vandermeirsch, F., Chaigneau, A., Pegliasco, C., Morrow, R., et al. (2016). An index to distinguish surface- and subsurface-intensified vortices from surface observations. Journal of Physical Oceanography, 46(8), 2529–2552. https://doi.org/10.1175/ JPO-D-15-0122.1

Assene, F. et al. (2020). From Mixing to the Large Scale Circulation: How the Inverse Cascade Is Involved in the Formation of the Subsurface Currents in the Gulf of Guinea, *Fluids*, *5*(3), 147, doi:10.3390/fluids5030147.

Athié, G & Marin, F. (2008). Cross-equatorial structure and temporal modulation of intraseasonal variability at the surface of the tropical Atlantic Ocean, J. Geophys. Res., 113, C08020, doi :1029/2007JC004332.

Benthuysen, J., Thomas, L. (2012). Friction and Diapycnal Mixing at a Slope: Boundary Control of Potential Vorticity. J. Phys. Oceanogr. 42, 1509–1523.

Bourlès, B., Gouriou, Y., Chuchla, R. (1999a). On the circulation in the upper layer of the western equatorial Atlantic. Journal of Geophysical Research 104, 21,151–21,170.

Chaigneau, A., Eldin, G. & Dewitte, B. (2009). Eddy activity in the four major upwelling systems from satellite altimetry (1992–2007), Prog. Oceanogr., 83(1–4),117–123, doi:10.1016/j. Pocean.2009.07.012

Chaigneau, A., Gizolme, A., & Grados, C. (2008). Mesoscale eddies off Peru in altimeter records: Identification algorithms and eddy spatio-temporal patterns, Prog. Oceanogr.,79(2–4), 106–119,doi:10.1016/j.pocean. 2008.10.013.

Chaigneau, A., Le Texier A., Eldin G., Grados C., and Pizarro O. (2011), Vertical structure of mesoscale eddies in the eastern South Pacific Ocean: A composite analysis from altimetry and Argo profiling floats, *Journal of Geophysical Research*, *116*(C11), doi:10.1029/2011jc007134.

Charney, J. G., & Stern, M. E. (1962). On the stability of internal baroclinic jets in a rotating atmosphere. Journal of the Atmospheric Sciences, 19(2), 159–172. https://doi.org/10.1175/1520 0469(1962)019<0159:OTSOIB>2.0.CO;2

Chelton, D. B., Schlax M. G., and Samelson R. M. (2011). Global observations of nonlinear mesoscale eddies, *Progress in Oceanography*, *91*(2), 167–216, doi:10.1016/j.pocean.2011.01.002.

Csanady, G. T. (1987), What controls the rate of equatorial warm water-mass formation? J. Mar. Res., 45, 513 – 532.

D'Asaro, E. A. (1988). Generation of submesoscale vortices: A new mechanism. Journal of Geophysical Research: Oceans, 93 (C6), 6685{6693.

Da-Allada, C. Y., Jouanno, J., Gaillard, F. et al. (2017). Importance of the equatorial undercurrent on the sea surface salinity in the eastern equatorial Atlantic in boreal spring. *J. Geophys. Res. Oceans* 122, 521–538. doi: 10.1002/2016JC012342

Dadou I., Garçon, V., Andersen, V. , FlierI, G. R., & Davis, C. S. (1996). Impact of the North Equatorial Current meandering on a pelagic ecosystem: A modeling approach, Journal of Marine Research, 54, 311-342

Delpech, A.; Cravatte, S.; Marin, F.; Morel, Y.; Gronchi, E.; Kestenare, E. (2020). Observed Tracer Fields Structuration by Middepth Zonal Jets in the Tropical Pacific. J. Phys. Oceanogr. 50, 281–304, doi:10.1175/JPO-D-19-0132.1.

Ducet N., Le Traon P.-Y., & Reverdun, G. (2000). Global high-resolution mapping of ocean circulation from TOPEX/Poseidon and ERS-1 and -2, J. Geophys. Res. 105 (C8), 19,477-19,498.

Emery, W. J. (2003), Water Types and Water Masses, Ocean Circulation, pp. 1556–1567, Elsevier Sci., Amsterdam, Netherlands

Emery, W.J., Meincke, J., (1986). Global water masses: summary and review. Oceanol. Acta 9 (4). 344-383.

Foussard, A., Lapeyre G. , and Plougonven R. (2019). Response of Surface Wind Divergence to Mesoscale SST Anomalies under Different Wind Conditions, *Journal of the Atmospheric Sciences*, *76*(7), 2065–2082, doi:10.1175/jas-d-18-0204.1.

Frenger, I., Gruber N. , Knutti R., and Münnich M. (2013). Imprint of Southern Ocean eddies on winds, clouds and rainfall, *Nature Geoscience*, *6*(8), 608–612, doi:10.1038/ngeo1863.

Garraffo, Z. D., Johns, W. E., Chassignet, E. P., & Goni, G. J. (2003). North Brazil Current rings and transport of southern waters in a high resolution numerical simulation of the North Atlantic. In G. J. Goni & P. Malanotte-Rizzoli (Eds.), Interhemispheric Water exchange in the Atlantic Ocean, Elsevier Oceanographic Series 68 (pp. 375–409). Amsterdam: Elsevier.

Gaube, P., Mcgillicuddy D. J., Chelton D. B. , Behrenfeld M. J. , and Strutton P. G. (2014). Regional variations in the influence of mesoscale eddies on near-surface chlorophyll, *Journal of Geophysical Research: Oceans*, *119*(12), 8195–8220, doi:10.1002/2014jc010111.

Gula, J., Molemaker M., McWilliams, J. (2015). Topographic vorticity generation, submesoscale instability and vortex street formation in the Gulf Stream. Geophys. Res. Lett. 42, 4054–4062.

Gula, J.; Molemaker, M.; McWilliams, J. (2016). Topographic generation of submesoscale centrifugal instability and energy dissipation. Nat. Commun. 7, 12811, doi:10.1038/ncomms12811.

Haynes, P., McIntyre, M. (1987). On the evolution of vorticity and potential vorticity in the presence of diabatic heating and frictional or other forces. J. Atmos. Sci. 44 (5), 828–841.

Herbette S., Morel Y. and Arhan M. (2004). Subduction of a Surface vortex under an outcropping front. J. Phys. Ocean. 34, pp. 1610-1627.

Herbette S., Morel Y. and Arhan M. (2003). Erosion of a surface vortex by a seamount. J. Phys. Oceanogr. 33, 1664– 1679

Holmes, R.M., Thomas, L.N. (2016). Modulation of Tropical Instability Wave Intensity by Equatorial Kelvin Waves. J. Phys. Oceanogr. 46, 2623–2643, doi:10.1175/JPO-D-16-0064.1.

Holmes, R.M., Thomas, L.N., Thompson, L., Darr, D. (2014). Potential Vorticity Dynamics of Tropical Instability Vortices. J. Phys. Oceanogr. 44, 995–1011, doi:10.1175/JPO-D-13-0157.1.

Hormann, V., and Brandt P. (2007). Atlantic equatorial undercurrent and associated cold tongue variability, J. Geophys. Res., 112, C06017, doi:10.1029/2006JC003931.

Hoskins, B.J., McIntyre, M. E., Robertson, A.W. (1985). On the use and significance of isentropic potential vorticity maps. Q. J. R. Met. Soc. 470, 877–946.

Kelly, B., Meyers S. , and O'Brien J. (1995). On a generating mechanism for Yanai waves and the 25-day oscillation, J. Geophys. Res., 100, 10,589 – 10,612.

Keppler, L., Cravatte S., Chaigneau A., Pegliasco C., Gourdeau L., and Singh A. (2018). Observed Characteristics and Vertical Structure of Mesoscale Eddies in the Southwest Tropical Pacific, *Journal of Geophysical Research: Oceans*, *123*(4), 2731–2756, doi:10.1002/2017jc013712.

Kirchner, K., Rhein M., Hüttl-Kabus S. , and Böning C. W. (2009). On the spreading of South Atlantic Water into the northern hemisphere. J. Geophys. Res., 114, C05019, doi:10.1029/ 2008JC005165

Kolodziejczyk, N., Bourlès B., Marin F., Grelet J., and Chuchla R. (2009). Seasonal variability of the Equatorial Undercurrent at 10°W as inferred from recent in situ observations, J. Geophys. Res., 114, C06014, doi:10.1029/2008JC004976.

Laxenaire, R., Speich S., Blanke B., Chaigneau, A., Pegliasco C., and Stegner A. (2018), Anticyclonic Eddies Connecting the Western Boundaries of Indian and Atlantic Oceans, *Journal of Geophysical Research: Oceans*, *123*(11), 7651–7677, doi:10.1029/2018jc014270.

Laxenaire, R., Speich, S., and Stegner, A. (2020). Agulhas ring heat content and transport in the South Atlantic estimated by combining satellite altimetry and Argo profiling floats data. Journal of Geophysical Research: Oceans, 125, e2019JC015511. https:// doi.org/10.1029/2019JC015511

Le Traon P.-Y., Nadal, F., and Ducet, N. (1998). An Improved Mapping Method of Multisatellite Altimeter Data,

J. Atmos. Oceanic Technol. 15, 522-534

Liu, M. and Tanhua, T. (2019). Characteristics of Water Masses in the Atlantic Ocean based on GLODAPv2 data, Ocean Sci. Discuss., https://doi.org/10.5194/os-2018-139, in review.

Locarnini, R. A., Mishonov, A. V., Baranova, O. K. et al. (2018). *World Ocean Atlas 2018, Volume 1: Temperature.* A. Mishonov Technical Ed.; NOAA Atlas NESDIS 81, 52 pp.

Martínez-Marrero, A., Rodríguez-Santana A., Hernández-Guerra A., et al., (2008). Distribution of water masses and diapycnal mixing in the Cape Verde Frontal Zone, Geophys. Res. Lett., 35, L07609, doi:10.1029/2008GL033229

McGillicuddy, D. J. (2016), Mechanisms of Physical-Biological-Biogeochemical Interaction at the Oceanic Mesoscale, *Annual Review of Marine Science*, *8*(1), 125–159, doi:10.1146/annurev-marine-010814-015606.

McWilliams, G. and Flierl, R. (1979). On the evolution of isolated, nonlinear vortices. J. Phys. Oceanogr., 9, 1155–1182.

Morel, Y. G., and McWilliams, J.C., (1997). Evolution of isolated interior vortices in the ocean, J. Phys. Oceanogr. 27, 727–748.

Morel, Y., Gula J., and Ponte A. (2019). Potential vorticity diagnostics based on balances between volume integral and boundary conditions, *Ocean Modelling*, *138*, 23–35, doi:10.1016/j.ocemod.2019.04.004.

Morel, Y., and McWilliams J. (2001). Effects of isopycnal and diapycnal mixing on the stability of oceanic currents. J. Phys. Oceanogr., 31, 2280–2296.

Morel, Y., Darr D., Tailandier, C., (2006). Possible sources driving the potential vorticity structure and long-wave instability of coastal upwelling and downwelling currents. J. Phys. Ocean. 36, 875– 896.

Morel, Y., Thomas, L. (2009). Ekman drift and vortical structures. Ocean Model. 27, 185–197

Morvan, M., L'Hégaret, P., Carton, X., Gula, J., et al., (2019). The life cycle of submesoscale eddies generated by topographic interactions. Ocean Science, 15, 1531– 1543. https://doi.org/10.5194/os-15-1531-2019

Pegliasco, C., Chaigneau, A., & Morrow, R. (2015). Main eddy vertical structures observed in the four major Eastern boundary upwelling systems: J. Geophys. Res. Oceans, 120, 6008- 6033.

Perez-Rodriguez, P., Pelegri, J. L., and Marrero-Diaz, A. (2001). Dynamical characteristics of the Cape Verde frontal zone, Sci. Mar., 65, 241–250.

Pujol, M.-I., Faugère, Y., Taburet, G., Dupuy, et al., (2016). DUACS DT2014: the new multi-mission altimeter data set reprocessed over 20 years, Ocean Sci., 12, 1067-1090.

Renault, L., Marchesiello, P., Masson, S., & McWilliams, J. C. (2019). Remarkable control of western boundary currents by Eddy Killing, a mechanical air-sea coupling process. Geophysical Research Letters, 46. https://doi.org/10.1029/2018GL081211

Saenko, O. A., Yang, D., & Gregory, J. M. (2018). Impact of mesoscale eddy transfer on heat uptake in an eddy-parameterizing ocean model. Journal of Climate, 31(20), 8589–8606. https://doi.org/10.1175/jcli-d-18-0186.1

Schuckmann, K. V., Brandt, P., and Eden, C. (2008). Generation of tropical instability waves in the Atlantic Ocean, *Journal of Geophysical Research*, *113*(C8), doi:10.1029/2007jc004712.

Schütte, F., Brandt, P., and Karstensen, J. (2016), Occurrence and characteristics of mesoscale eddies in the tropical northeastern Atlantic Ocean, *Ocean Science*, *12*(3), 663–685, doi:10.5194/os-12-663-2016.

Seo, H., Miller, A., and Norris, J. (2016), Eddy-wind interaction in the California current system: Dynamics and impacts, J. Phys. Oceanogr., 46, 439–459, doi:10.1175/JPO-D-15-0086.1.

Snowden, D., and Molinari, R. (2003), Subtropical cells in the Atlantic Ocean: An observational summary, in Interhemispheric Water Exchange in the Atlantic Ocean, edited by G. Goni and P. Malanotte-Rizzoli, Elsevier Oceanogr. Ser., 68, 287 – 312.

Sprintall, J., Tomczak, M. (1993). On the formation of central water in the southern hemisphere. Deep- Sea Research 40, 827—848.

Stramma, L., and Schott, F. (1999). The mean flow field of the tropical Atlantic Ocean, Deep Sea Res. II, 46, 279 – 303.

Stramma, L., Juttl S., and Schafstall, J. (2005a), Water masses and currents in the upper tropical northeast Atlantic off northwest Africa, J. Geophys. Res., 110, C12006, doi:10.1029/2005JC002939.

Stramma, L., Rhein, M., Brandt, P., et al. (2005b). Upper ocean circulation in the western tropical Atlantic in boreal fall 2000, Deep Sea Res., Part I, 52, 221 – 240, doi:10.1016/ j.dsr.2004.07.021.

Sutyrin G. G. and Flierl, G. R. (1994). Intense vortex motion on the beta-plane: development of the beta-gyres, J. Atmos. Sci. 51, 773–790

Sutyrin G.G. and Morel, Y.G. (1997). Intense vortex motion in a stratified fluid on the beta-plane: an analytical theory and its validation, J. Fluid Mech. 336, 203–220.

Sverdrup, H.U., Johnson, M.W., Fleming, R.H. (1942). The Oceans. Their Physics, Chemistry, and General Biology. Prentice-Hall, Englewood Cliffs, NJ, 1087 pp.

Thomas, L.N. (2015) Destruction of Potential Vorticity by Winds. J. Phys. Oceanogr., 35, 2457–2466, doi:10.1175/JPO2830.1.

Thomas, M. D., and Zhai, X. (2013). Eddy-induced variability of the meridional overturning circulation in a model of the North Atlantic, Geophys. Res. Lett., 40, 2742–2747, doi:10.1002/grl.50532

Tiedemann, M., Fock, H. O., Döring, J., Badji, L. B. and Möllmann, C. (2018) Water masses and oceanic eddy regulation of larval fish assemblages along the Cape Verde frontal zone. J. Mar. Syst., 183, 42–55.

Tomczak, M., Godfrey, J.S. (1994). Regional Oceanography: An Introduction. Elsevier, Oxford, 422 pp.

Tsuchiya, M., Talley, L. D., and McCartney, M. S. (1992). An eastern Atlantic section from Iceland southward across the equator, Deep Sea Res., 39, 1885 – 1917

Urbano, D. F., De Almeida, R. A. F., and Nobre, P. (2008). Equatorial Undercurrent and North Equatorial Countercurrent at 38°W: A new perspective from direct velocity data. J. Geophys. Res., 113, C04041, doi:10.1029/2007JC004215

Vandermeirsch, F., Morel, Y., and Sutyrin, G. (2001). The net advective effect of a vertically sheared current on a coherent vortex. J. Phys. Oceanogr., 31, 2210–2225.

Villas Bôas, A. B., Sato, O. T., Chaigneau, A. and Castelão, G. P. (2015). The signature of mesoscale eddies on the air-sea turbulent heat fluxes in the South Atlantic Ocean, *Geophysical Research Letters*, *42*(6), 1856–1862, doi:10.1002/2015gl063105.

Wang, C. (2005). Subthermocline tropical cells and equatorial subsurface countercurrents. Deep Sea Res. Part Oceanogr. Res. Pap. 52, 123–135, doi:10.1016/j.dsr.2004.08.009.

Weisberg R. H., Weingartner, T. J. (1988). Instability waves in the equatorial Atlantic Ocean Journal of Physical Oceanography, 18, pp. 1641-1657

Wilson, W., Johns, E., and Molinari, R. (1994). Upper layer circulation in the western tropical North Atlantic Ocean during August 1989, J. Geophys. Res., 99, 22,513 – 22,523.

Zenk, W., B. Klein, and Schröder, M. (1991). Cape Verde Frontal Zone, Deep Sea Res., 38, suppl. 1, S505-S530

Zweng, M. M., Reagan, J. R., Seidov, D. et al. (2018). *World Ocean Atlas 2018, Volume 2: Salinity.* A. Mishonov Technical Ed.; NOAA Atlas NESDIS 82, 50 pp.

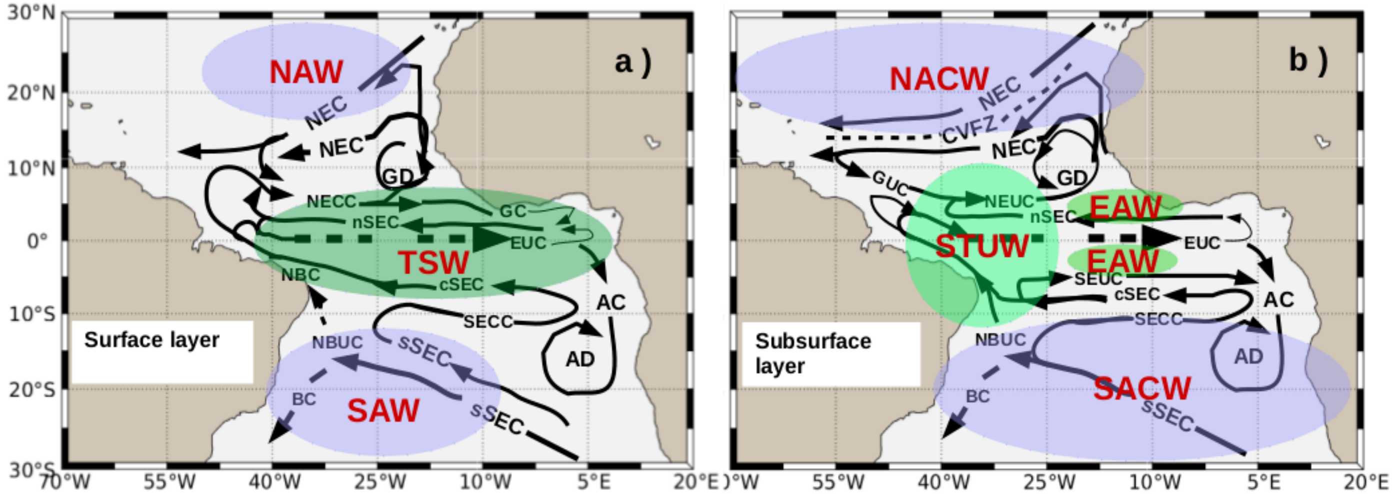

Figure1: Schematic view of **a)** surface and **b)** subsurface circulation in the TAO (adapted from Stramma and Schott, 1999). Main currents are: Brazil Current (BC), North Brazil Current (NBC), North Brazil Undercurrent (NBUC), North Equatorial Current (NEC), North Equatorial Countercurrent (NECC), northern, central and southern branches of South Equatorial Current (nSEC, cSEC, sSEC), Guinea Current (GC), Angola Current (AC), Angola Dome (AD), Guinea Dome (GD), South Equatorial Countercurrent (SECC), Equatorial Undercurrent (EUC), North Equatorial Undercurrent (NEUC), South Equatorial Undercurrent (SEUC), Guiana Undercurrent (GUC). Tropical surface water-masses and central water-masses are also indicated: Tropical Surface water (TSW), Northern, southern and eastern tropical Atlantic water (NAW, SAW, EAW), Subtropical Underwater (STUW), North and South Atlantic Central Water (NACW, SACW).

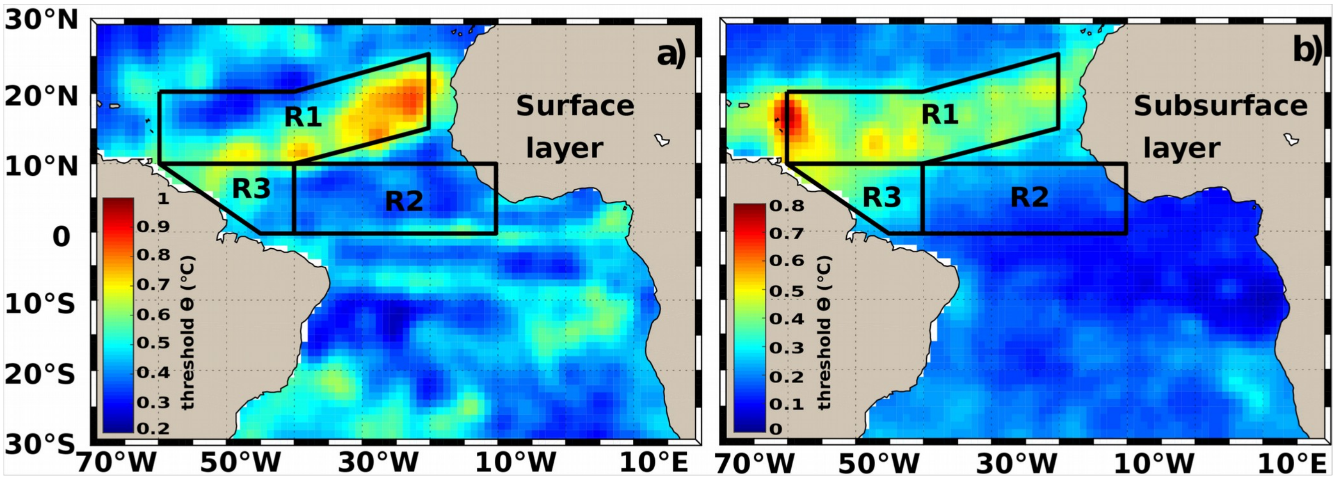

Figure2: Annual mean of the isopycnal temperature anomaly threshold within the **a)** surface and **b)** subsurface layers. Three dynamically different subregions (R1, R2, R3) used in this study are delimited in black (see in-text description of these regions). Surface layer extends from the surface to the base of the pycnocline, whereas subsurface layer extends below the thermocline to 1000 m depth.

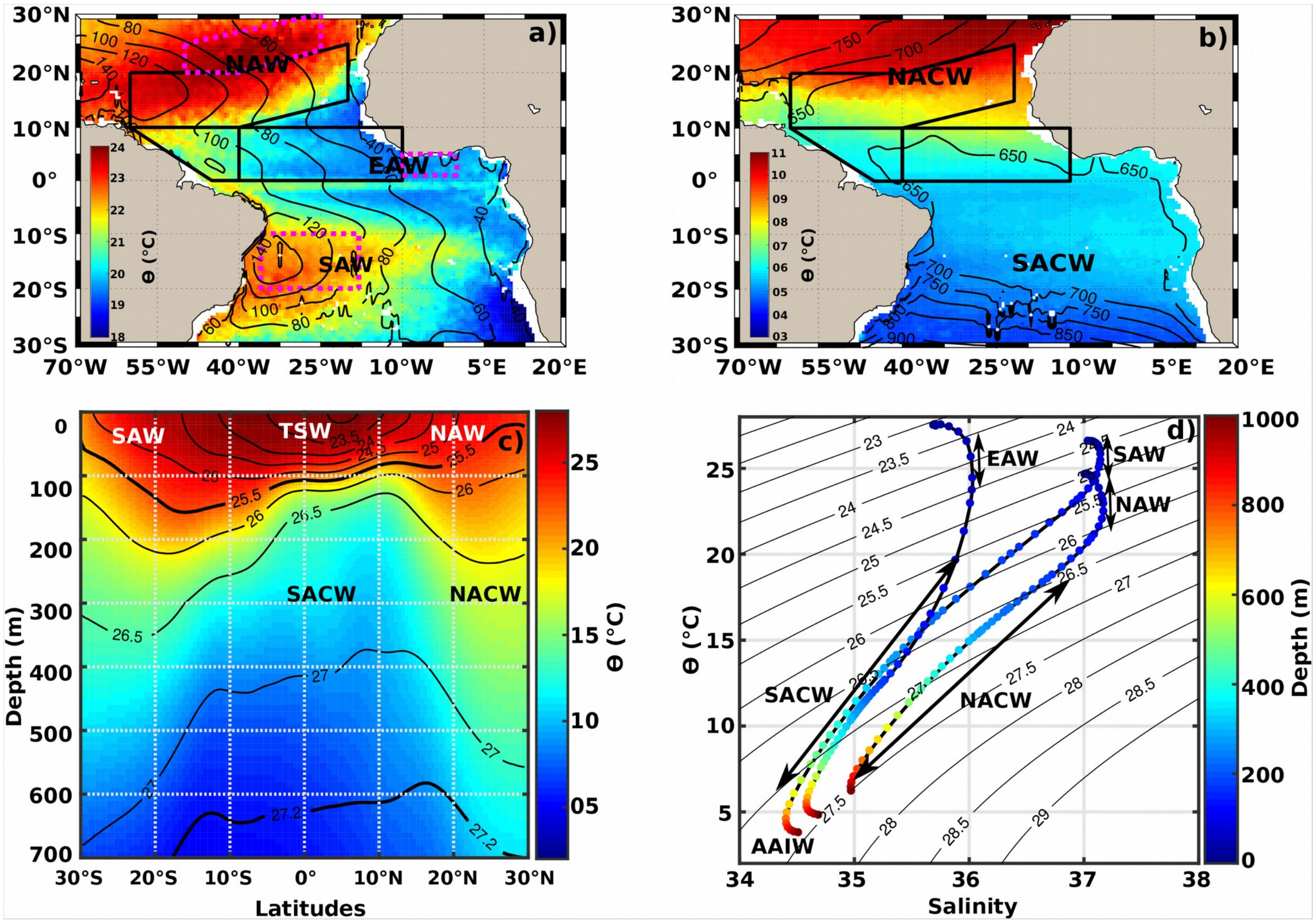

Figure 3: Large-scale temperature distribution (in °C) on **a)** $\sigma_\theta = 25.5$ kg.m^{-3} and **b)** $\sigma_\theta = 27.2$ kg.m^{-3}. Black contours correspond to the depth (in m) of the corresponding σ_θ layer, whereas black boxes delimits the R1-R3 subregions. **c)** Mean meridional temperature section along 35°W; black contours depict σ_θ levels. **d)** Mean Θ-*S* diagram and main water-masses observed within the 3 magenta boxes delimited in a]. Water-masses: NAW: North Atlantic Water; SAW: South Atlantic Water; TSW: Tropical Surface Water; EAW: Eastern Atlantic Water; NACW: North Atlantic Central Water; SACW: South Atlantic Central Water; AAIW: Antarctic Intermediate Water.

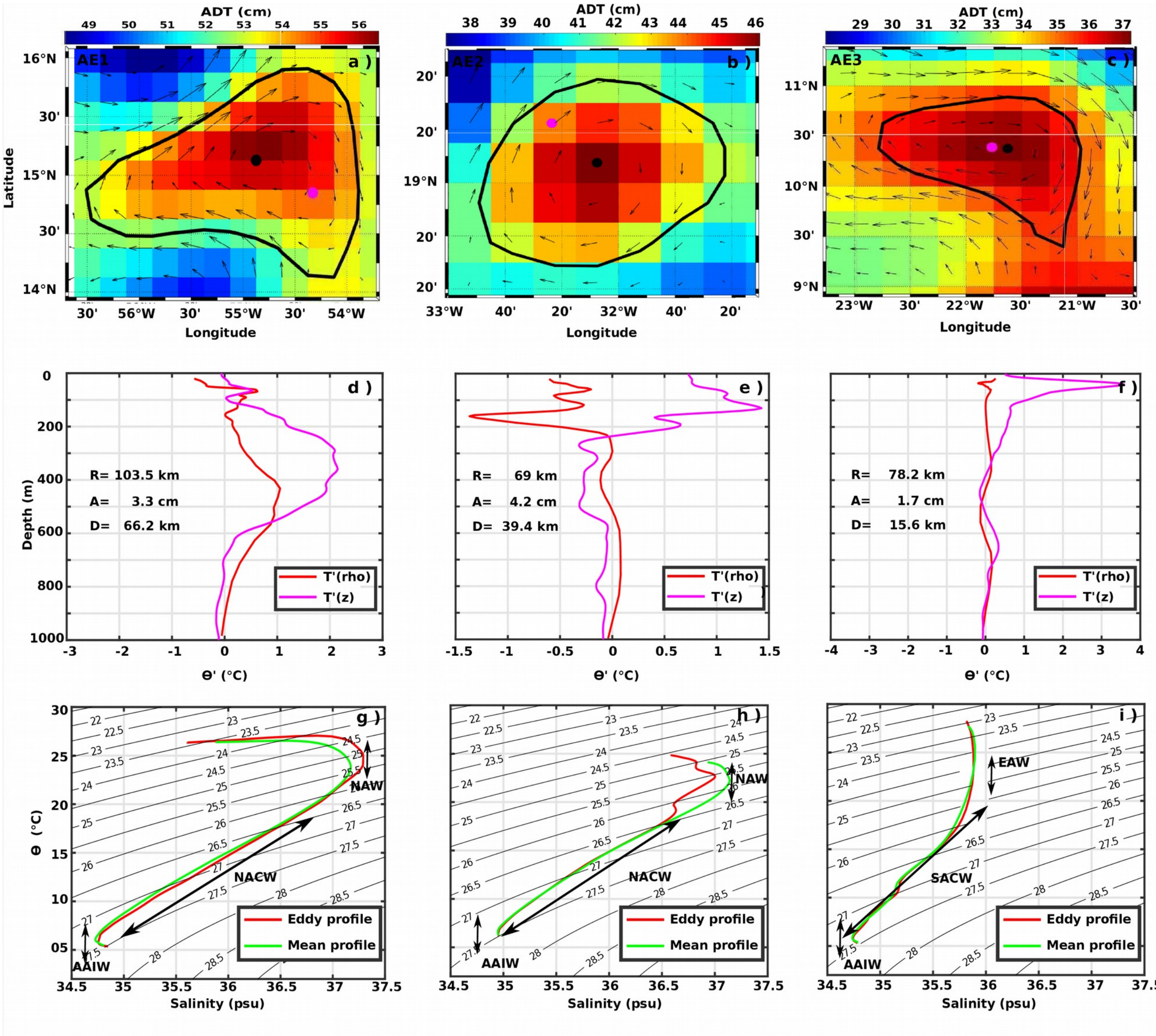

Figure 4: Density-coordinate anomalies compared to depth-coordinate anomalies for three case-study anticyclonic eddies. **a-c)** Eddy characteristics in AVISO maps. Black and magenta dots correspond to the eddy centers and the location of surfaced Argo floats, respectively, whereas black contours delimit eddy edges. **d-f)** Temperature anomalies observed within eddies in depth-coordinates (magenta lines) and in density-coordinates (red lines) re-projected on depths. R, A and D indicate the eddy radius, amplitude and the distance of the surfaced Argo float to the eddy center. **g-i)** Θ-S diagram obtained within eddies (red lines) and for the mean climatology at the same location (green curves). Water-masses: NAW: North Atlantic Water; EAW: Eastern

Atlantic Water; NACW: North Atlantic Central Water; SACW: South Atlantic Central Water; AAIW: Antarctic Intermediate Water.

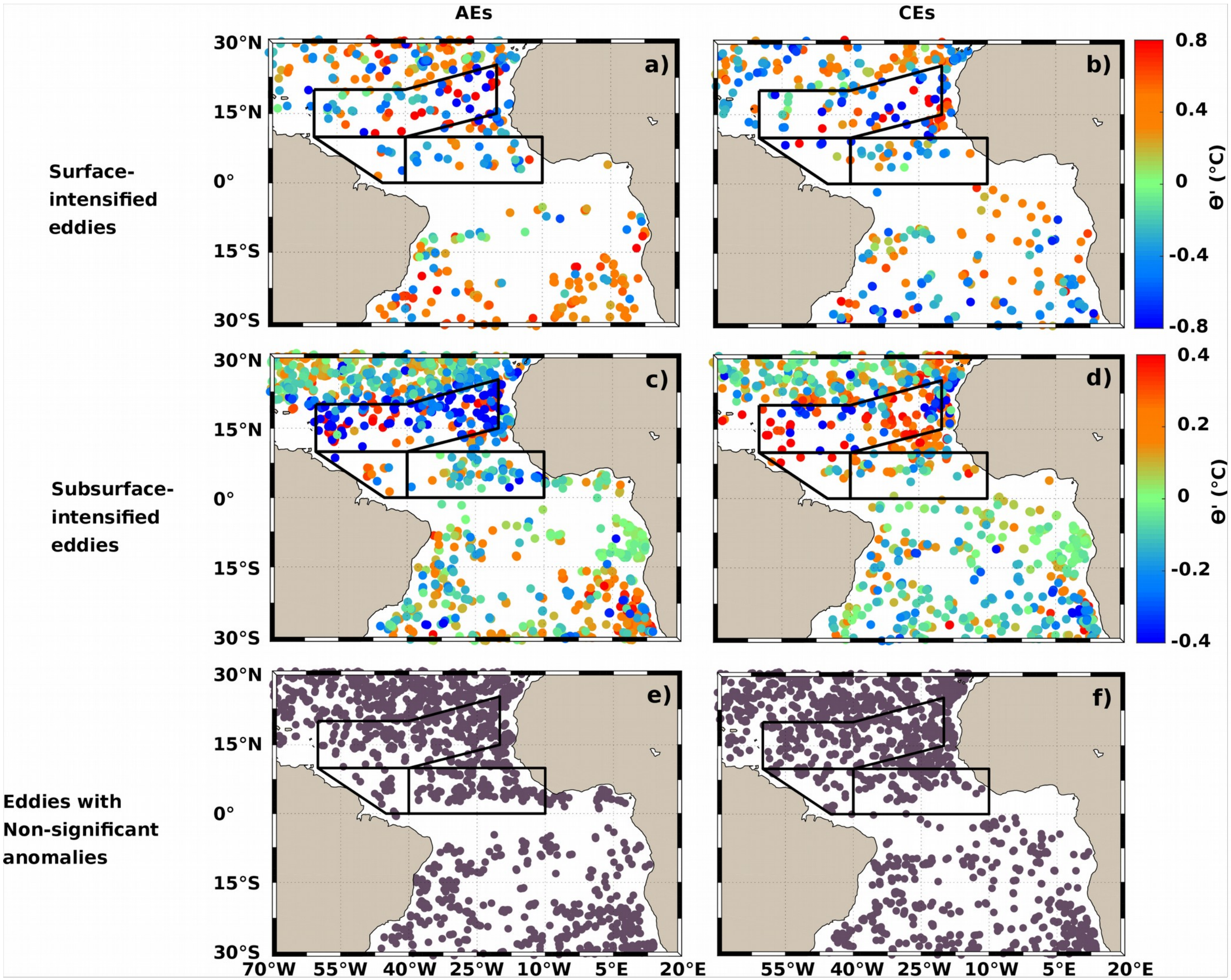

Figure 5: Spatial distribution of significant **a-b)** surface and **c-d)** subsurface temperature anomalies in anticyclonic (**AEs**, left column) and cyclonic (**CEs**, right column) eddies. **e-f)** Spatial distribution of new-born eddies having non-significant isopycnal anomalies. Black boxes delimit the R1-R3 subregions.

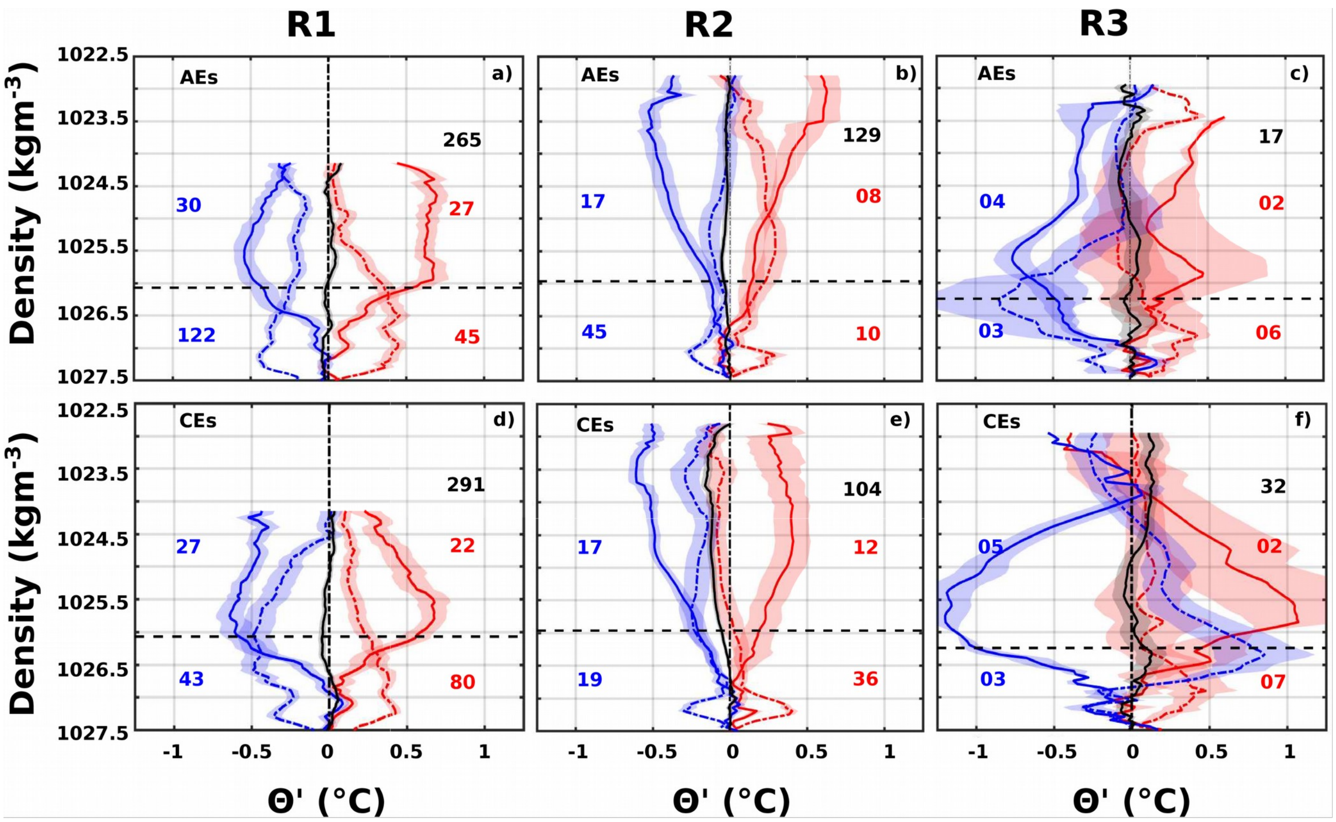

Figure 6: Mean isopycnal temperature structures of **a-c)** Anticyclonic (AEs) and d-f) Cyclonic (CEs) new-born eddies within 3 sub-regions. Surface and subsurface intensified anomalies are represented in solid and dashed lines respectively, whereas positive anomalies are in red and negative anomalies in blue. Non-significant anomalies are represented in black. For each subplot, black numbers indicate the number of eddies having non-significant Θ', the right red top (bottom, respectively) numbers indicate the number of surface (subsurface) intensified-eddies with positive anomalies and the left blue top (bottom, respectively) numbers indicate the number of surface (subsurface) intensified eddies with negative anomalies. R1-R3 are the defined subregions.

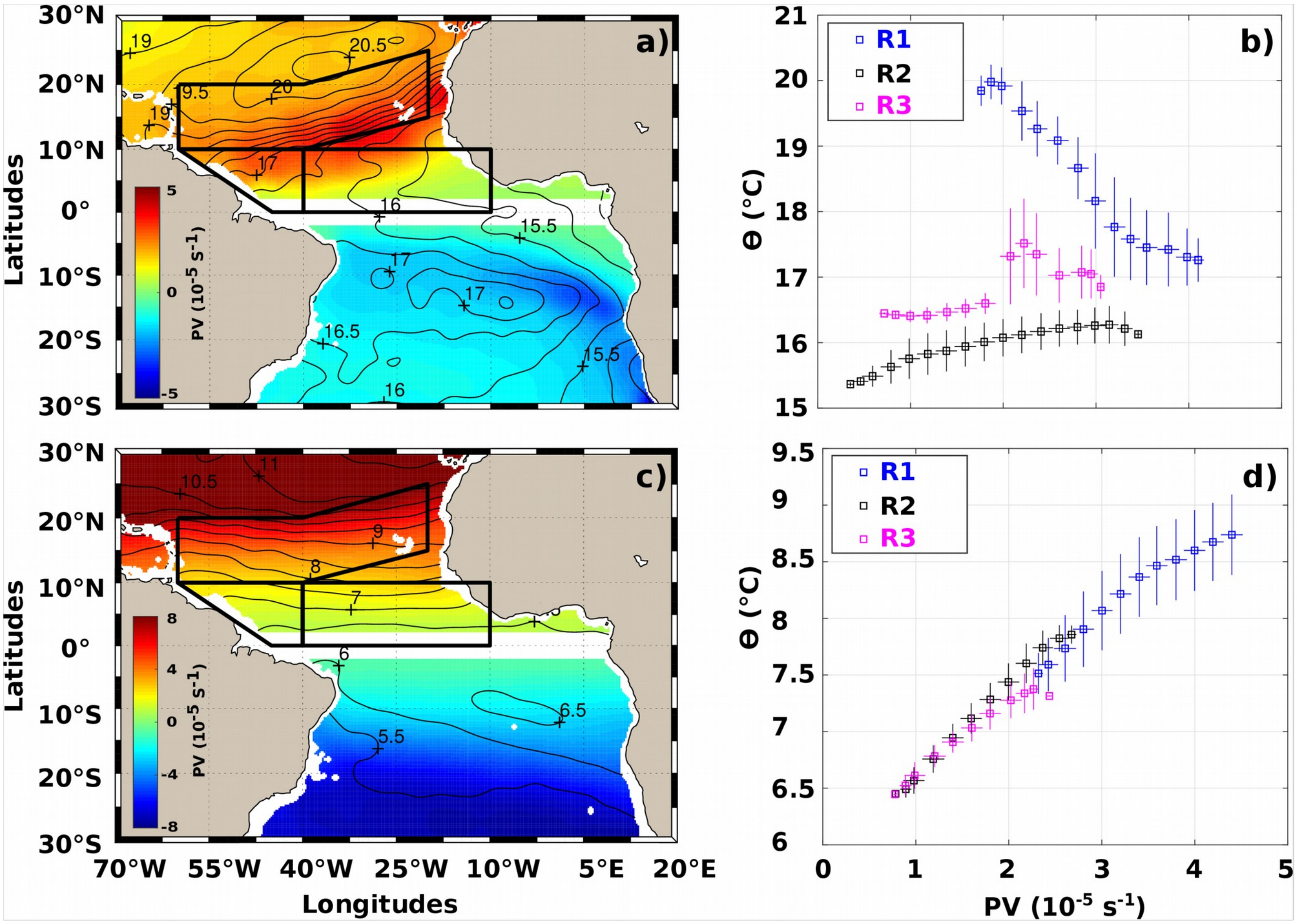

Figure 7: Large-scale rescaled potential vorticity (PV, color shading) and Θ (in °C, black contours), averaged between **a)** $\sigma_\theta = 25.75 - 26.5$ kg.m^{-3} and **c)** $\sigma_\theta = 26.9 - 27.4$ kg.m^{-3}. Black boxes delimit the R1-R3 subregions. **b & d)** PV- Θ relationships in R1-R3 subregions. PV (and corresponding Θ) were averaged in intervals of 0.2 10^{-5} s^{-1} (dots) and the corresponding standard deviations are indicated by solid lines.

Table1: Number of eddies with significant and non-significant anomalies in the TAO. The corresponding percentages are indicated between brackets.

		Northern Hemisphere					**Southern Hemisphere**				
		Positive anomalies	Negative anomalies	Non-significant anomalies	Ratio significant/ non-significant	Ratio Subsurface/ surface	Positive anomalies	Negative anomalies	Non-significant anomalies	Ratio significant/ non-significant	Ratio Subsurface/ surface
AEs	surface-intensified	151 (6.79%)	131 (5.89%)	1124 (50.52%)	0.98	2.90	130 (11.97%)	28 (2.58%)	474 (43.65%)	1.29	2.87
	Subsurface -intensified	359 (16.13%)	460 (20.67%)				282 (25.97%)	172 (15.84%)			
CEs	surface-intensified	130 (6.90%)	121 (6.43%)	1100 (58.42%)	0.82	2.58	75 (6.78%)	93 (8.41%)	475 (42.95%)	1.33	2.75
	Subsurface -intensified	422 (22.41%)	227 (12.06%)				202 (18.26%)	261 (23.60%)			